Journal of Materials Chemistry C

RSC Publishing

PAPER

View Article Online
View Journal | View Issue

Cite this: J. Mater. Chem. C, 2013, 1, 1990

A theoretical study of the dielectric and magnetic responses of Fe-doped α-MnO_2 based on quantum mechanical calculations

Yuping Duan,* Zhuo Liu, Yahong Zhang and Ming Wen

Received 31st October 2012
Accepted 10th January 2013

DOI: 10.1039/c3tc00902e

www.rsc.org/MaterialsC

The microwave electromagnetic properties of Fe-doped α-MnO_2 are studied theoretically using quantum mechanical calculations based on density functional theory. The calculations employ the Perdew–Burke–Ernzerhof model, a generalized gradient approximation, to deal with the exchange–correlation interaction. The possible role of Fe doping in modifying the electromagnetic performance is studied utilizing density of states (DOS) and the bond length between the metal and oxygen. Calculations of the bond length in the presence of Fe show a contracted bond length between the metal atoms and O with enhanced bond strength, resulting in increased storage of electric field energy. This explains the experimental observation of a reduced dielectric loss after Fe-doping. The DOS results demonstrate that Fe doping enhances the spin-polarization of MnO_2. Therefore, the total magnetic moment is increased after doping, corresponding to the magnetic enhancement of MnO_2. The theoretical predictions concluded from the quantum mechanical calculations agree well with the experimental observations. The results provide an early stage exploration of theoretical research on the microwave absorbing properties of doped MnO_2.

1 Introduction

Manganese dioxide compounds have been the subject of experimental and theoretical investigations due to their adjustable physical and chemical performance. Since the first report of MnO_2 as a microwave absorbent,[1] the rational design and fabrication of MnO_2 absorbents together with their derivatives have attracted increasing attention due to its strong dielectric loss and controllable crystal structures.[2–4] In the studies of electromagnetic absorbents, the dielectric loss and magnetic loss properties are the principal focus. The strong dielectric losses exhibited by MnO_2 are generally attributed to the dominant dipolar polarization, interfacial polarization and the associated relaxation phenomena. In terms of magnetism, MnO_2 is classified as a type of antiferromagnetic or paramagnetic material with a negligibly small magnetic loss. Recently, our group[5] reported that appropriate Fe-doping could effectively enhance the magnetic loss of MnO_2, in which the spin-glass behavior was proposed as the mechanism for magnetic loss. Up to now, the experimental research on MnO_2 in various fields has been relatively extensive.[6] However, these studies mostly focused on the experimental synthesis of MnO_2 with novel morphologies, of which the microscopic mechanism is still vague to some degree. Thus, a consistent and rigorous theoretical description of its electromagnetic properties remains a fundamental challenge for further development of MnO_2 absorbing materials.

Mn is known to be one of the most complex metallic elements due to its special electronic configuration in the 3d orbital. The majority 3d orbitals are completely filled with five electrons, while the minority 3d orbitals are all left empty. This would inevitably impact the magnetic coupling states of the Mn atoms in different valences, so the magnetic arrangements vary with the different oxidation states of Mn.[7] It has also been established that the bond length of Mn–Mn is the other decisive factor in the magnetic couplings between Mn atoms.[8,9] These reasons make Mn-based materials display intriguing electromagnetic performance. Theoretical calculations based on quantum mechanics are blocked by the complex coupling among Mn atoms, so the work in this aspect is not fully understood.[7,10]

Manganese dioxides crystallize in a wide range of structures with flexible building methods *via* the edge-shared or corner-shared [MnO_6] octahedra. One such example, α-MnO_2, has been widely used in microwave absorbing and many other applications due to its unique 2 × 2 tunnel structures with a pore size of about 4.6 Å. The tunnels offer the possibility of the incorporation of cations (K^+, NH^{4+}, Ba^{2+}, *etc.*) and a small number of water molecules. To maintain electrostatic equilibrium, when the intentional impurity ions replace Mn^{4+} ions in the octahedral centers, the concentration of the above cations is self-regulated. As a result, the additional cations

School of Materials Science and Engineering, Dalian University of Technology, Dalian 116085, P. R. China. E-mail: duanyp@dlut.edu.cn; Fax: +86 411 84708446; Tel: +86 411 84708446

perform an important stabilization function for the tunnel structure of α-MnO_2, and influence its corresponding properties at the same time. Therefore, α-MnO_2 has the capacity to be a potential doping target by ion-exchanging, both in the tunnels and in the centers of octahedra. So far, various cations (Fe^{3+}, Cr^{3+}, Ag^{+}, *etc.*) have been introduced as dopants into α-MnO_2 structures,[11–13] but the nature of the doping cations is still uncertain. Research has shown that doping ions are very likely to substitute a small amount of the original ions due to similar ionic radii or closed valance states compared with the original ions.[14,15] So in this preliminary theoretical study, the doping of Fe is processed as an ionic substitution.

In this paper, the first-principles calculations are performed within a computational framework to study the Fe doping effect on the electronic states of α-MnO_2, and hence further the understanding of the electromagnetic wave absorbing mechanisms of α-MnO_2. To our best knowledge, this work has not been reported before. It is found that this theoretical method throws light on the rational design of new functional materials.

2 Method and computational details

The MnO_2 models for calculations are constructed as follows. The undoped MnO_2 model is an ideal α-MnO_2 supercell ($2 \times 1 \times 1$, $Mn_{16}O_{32}$), as shown in Fig. 1(a). The Fe-doped MnO_2 model ($Mn_{15}FeO_{32}$) is built by replacing one of the Mn atoms with an Fe atom based on the undoped MnO_2 model, as shown in Fig. 1(b). The corresponding doping concentration by molar ratio is 6.25%. It should be noted that the outer electronic configurations of Mn, Fe and O atoms are $3d^5 4s^2$, $3d^6 4s^2$ and $2s^2 2p^4$, respectively. Both Mn and Fe are magnetic atoms. Therefore the magnetic arrangement of the Mn atoms is considered, and the ground-state magnetic structure of α-MnO_2 is built as in ref. 16: the Mn–Mn coupling between corner-sharing [MnO_6] is antiferromagnetic, while the coupling between edge-sharing [MnO_6] is ferromagnetic, as shown in Fig. 1. The calculation process is conducted in two steps: geometry optimization and energy calculation.

The first-principles calculations are carried out using the CASTEP code,[17] using the density functional theory (DFT) framework based on the plane wave basis set and the ultrasoft pseudopotential.[18,19] The Perdew–Burke–Ernzerhof (PBE) parameterization utilizing generalized-gradient approximation (GGA) scheme is adopted to deal with the exchange–correlation interactions.[20] To overcome the limitations of the conventional GGA, for example the underestimation of the band gap, a Coulomb correction of $U = 2.5$ eV is induced. Considering both the calculation efficiency and accuracy, structural geometries and forces are well-converged for a $1 \times 3 \times 9$ Monkhorst–Pack grid with a cutoff energy of 340 eV. The total energy is converged to 1.0×10^{-6} eV per atom. A Gaussian smearing of 0.1 eV was used for the Fermi surface broadening. Relaxations of atomic positions and lattice vectors were performed until residual forces were 0.03 eV $Å^{-1}$ or less. The whole calculation process is carried out in the reciprocal space.

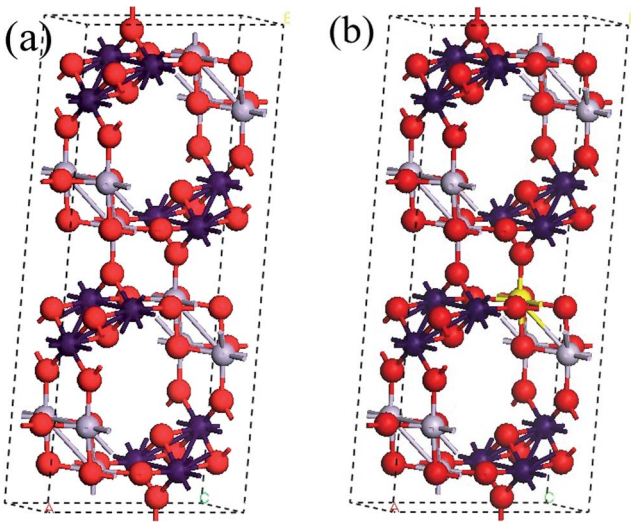

Fig. 1 The constructed model of (a) pure and (b) Fe-doped α-MnO_2. Mn atoms in spin-up states are represented by dark purple spheres, Mn atoms in spin-down states by light purple spheres, O atoms by red spheres, and the Fe atom by a yellow sphere.

3 Results and discussion

3.1 Microwave dielectric properties

The dielectric properties of a structured model can be directly obtained *via* the first-principles calculation based on DFT. However, the frequency range is limited to optical frequencies with a significant error in microwave frequencies. This means the microwave dielectric functions cannot be calculated directly. The dielectric properties are strongly dependent on the crystal characteristics of the constitutent ions due to the nature of the materials. Researches have shown that the covalency of M–O (M represents a metal atom) bonds in the [MO_6] octahedra plays an important role in the microwave dielectric properties of the materials.[21–24] According to the bond valence theorem reported by Brown's group,[25,26] the covalency of the M–O bonds can be estimated, and both the bond strength and covalency of M–O are changed by the substitution of the original metal ions. Moreover, it is considered that the covalency of the M–O bond determines the strength of the macroscopic polarizability, and hence the dielectric performance. Li *et al.*[24] prepared $(1 - x)$

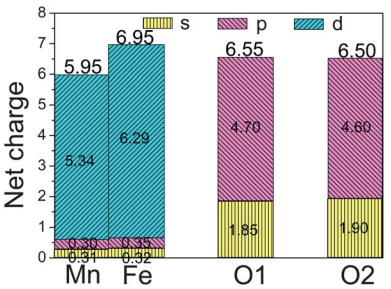

Fig. 2 The atomic population of pure and Fe-doped MnO_2 in each orbital. The influence of doping is mainly ascribed to the increased net charge of Fe in the 3d shell.

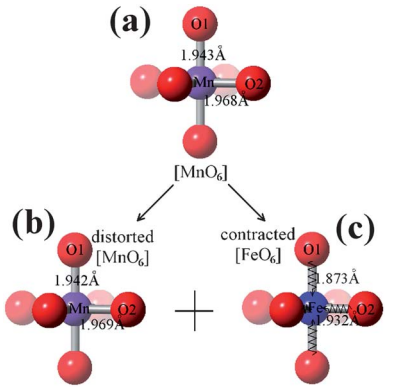

Fig. 3 The original octahedral [MnO_6] in pure-MnO_2 (a) is changed to the distorted [MnO_6] (b) and the contracted [FeO_6] (c) after Fe doping. The bond lengths of M–O decrease after Fe doping.

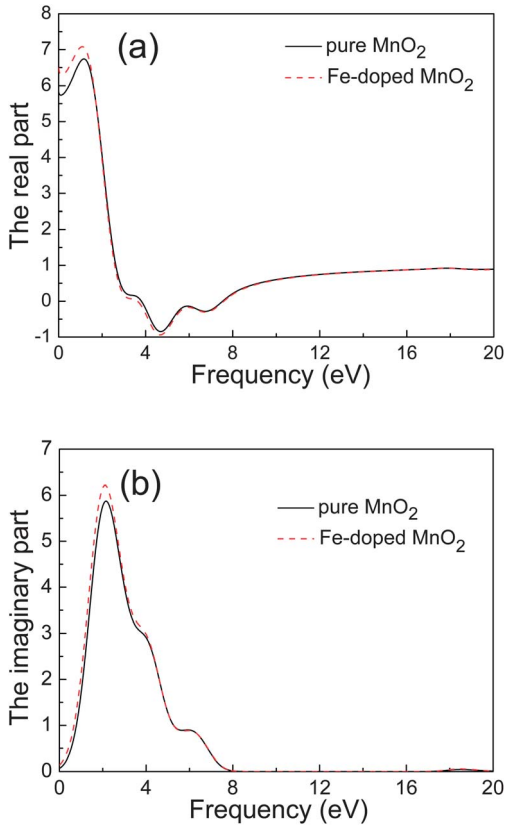

Fig. 4 The calculated dielectric functions at optical frequencies: (a) the real part of the dielectric function derived from the Kramers–Kronig transform; (b) the imaginary part calculated directly by direct evaluation of the matrix elements between the occupied and unoccupied electronic states.

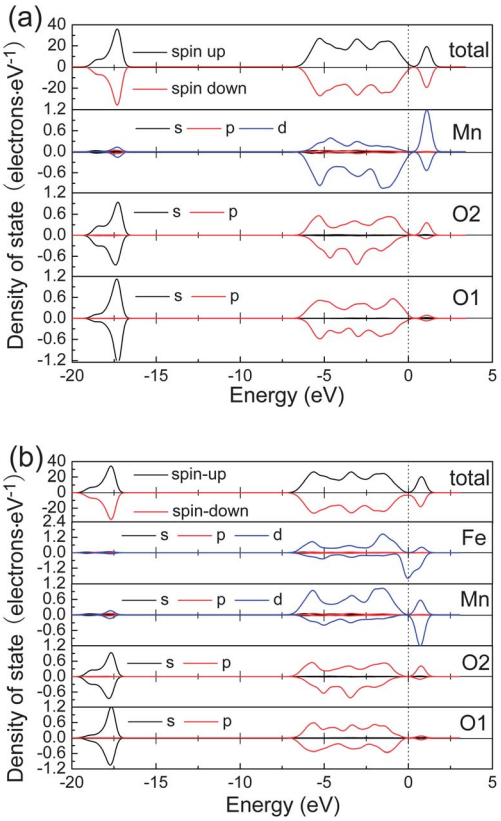

Fig. 5 The total and partial DOS of (a) pure and (b) Fe-doped α-MnO_2. The Fermi energy is expressed by the perpendicular dotted line.

Table 1 The net spin magnetic moment of pure and Fe-doped MnO_2

System	Mn	O1	O2	Fe	Total
Pure MnO_2	0	0	0	—	1.244×10^{-6}
Fe-doped MnO_2	−1.49	−0.11	0.01	0.85	−0.9995

$CaTiO_{3-x}(Li_{0.5}La_{0.5})O_3$ perovskite ceramics by a solid state reaction method, and reported that the dielectric property trends were in line with the bonding characteristics: the stronger covalency of M–O corresponded to a decreased dielectric constant and dielectric loss. The detailed reaction process is described as follows. When the external electromagnetic field is applied, the displacement polarization of electrons and ions is induced, which is reflected in the change to the bond length and bond angle. These changes are achieved through bond vibration: the polarization process enforces the affected ions into an anharmonic interaction, thus altering the vibration frequency. This process leads to the transformation of electric energy into lattice vibration energy, which contributes to the dielectric loss. Therefore the bonding between the metal and oxygen in transition metal oxides plays a decisive role in the dielectric properties. The high strength of the M–O covalent bond decreases the response damping to the applied field, so the dielectric attenuation caused by polarization is reduced.

The atomic net charges and bond lengths of the pure and Fe-doped MnO_2 are summarized in Fig. 2 and Fig. 3 respectively. To further understand the mechanism of the microwave dielectric performance, these parameters, containing the information of the covalent interactions, are discussed in turn. The calculation results indicate that the Mn ions in pure MnO_2 have an average positive charge of +1.05*e*, which means they are poor electron donors. There are two types of O atom according

to the calculated atomic charges after the geometry optimization, denoted as O1 and O2, and the numbers of the two types of O atom are in a 1 : 1 ratio. The net charges of O1 and O2 are $-0.55e$ and $-0.50e$, respectively. The difference in electronegativity between O1 and O2, which are both covalently bonded with Mn ions, is small. Fe doping has no effect on the positive charge of the Mn ions, *i.e.* $+1.05e$, which is consistent with the charge of the Mn ions in pure MnO_2. The net charge of the incorporated Fe ion is also $+1.05e$. The calculation results also reflect that, with respect to atomic population, the influence of doping is mainly attributed to the increased positive charge of Fe in the third shell, as shown in Fig. 2. From Fig. 3, it can be seen that the Mn–O bond length is changed slightly with Fe doping: the bond length of Mn–O1 is decreased by 0.001 Å, and Mn–O2 is increased by 0.001 Å. The lengths of the Fe–O bonds are shorter than those of the Mn–O bonds, as indicated in Fig. 3. This shows that the incorporation of Fe induces a lattice distortion, which shortens the bond lengths of the constructed system.

Therefore, Fe doping can result in the shortened bond length and an increased degree of overlap within the M–O covalent bond, hence the enhanced bond strength. So the potential energy of bonding is increased to store more electric field energy, and almost all of this energy is released once the applied electric field is removed. As the dielectric loss is expressed by the ratio of attenuated electric energy to stored electric energy, this increased energy storage corresponds to the decreased dielectric loss. Therefore, Fe doping reduces the dielectric loss of MnO_2. This theoretical prediction agrees well with previous experimental results.[4]

Furthermore, the dielectric functions at optical frequencies have also been calculated, and are shown in Fig. 4(a) and (b). The imaginary part of the complex permittivity is calculated numerically by direct evaluation of the matrix elements between the occupied and unoccupied electronic states, while the real part is calculated using the Kramers–Kronig transform.[27] In this calculated dielectric function, there are certain limitations, such as the neglection of the local field effect and the phonon contribution to the optical spectra. However, it can be used to explain the variation tendency after doping. From Fig. 4 it can be seen that both the real and imaginary parts for Fe-doped MnO_2 are slightly larger than that of pure MnO_2 at lower frequencies. When the frequency is further increased, the doping effect on dielectric performance is not obvious. There are several fluctuations at frequencies below 8.0 eV, and the imaginary parts at this frequency range are non-zero, which can be ascribed to the absorption spectrum. It should be noted that, compared to the reduced dielectric function after Fe-doping at microwave frequencies, the dielectric function predicted by theoretical calculations exhibits the opposite variation. This phenomenon is expected because different polarization mechanisms work at different frequency ranges.

3.2 Magnetism

The magnetic properties of a material are mainly determined by magnetic moments resulting from the orbiting and spinning of electrons around the nucleus. Therefore, the magnetism of doped α-MnO_2 can be analyzed by calculating the spin density. Fig. 5(a) and (b) show the density of states (DOS) of the pure and Fe-doped MnO_2, respectively. The Fermi energy is expressed by the perpendicular dotted line. It can be seen from Fig. 5 that the valance bands of pure and Fe-doped MnO_2 consist mainly of two parts. The upper valance band from -7 eV to 0 eV is contributed by the Mn 3d, O 2p, and Fe 3d states, while the lower valance band from -19.5 eV to -16.5 eV is dominated by the O 2s states. The localized density state indicates strong hybridization among Mn 3d, O 2p, and Fe 3d orbitals. Owing to the hybrid orbitals, stabilized chemical bonds are formed between the metal atoms and oxygen atoms. The spin-up and spin-down states in the DOS of pure MnO_2 exhibit a symmetrical distribution, as shown in Fig. 5(a). As for the Fe-doped MnO_2, however, Fe doping leads to the asymmetrical distribution in the total spin electronic partial density of states (PDOS) at the conduction band near the Fermi energy shown in Fig. 5(b), which is absent in that of Ni/Co-doped MnO_2 as reported in ref. 16. This specific distribution of the spin state indicates that the doped α-MnO_2 possesses enhanced magnetic characteristics.

As a result, in its calculation it is supposed that MnO_2 has weak magnetic performance, because the spin up and spin down partial DOS's of Mn in MnO_2 are not equal. However, it should be noted that this is just the theoretical calculation result. While considering the experimental situation, this magnetic ordering at room temperature is expected to be only short-range, and the thermal fluctuation above a particular temperature would readily randomize the magnetic interactions of Mn–Mn to some degree. So the practically measured complex permeability of α-MnO_2 exhibited nonmagnetic character.

In the exported calculation results, the value of the integrated spin density ($\times 2$) for pure MnO_2 is 1.2443×10^{-6}, while the absolute value of the integrated spin density ($\times 2$) is 49.8344. As for Fe-doped MnO_2, the former value is -0.9995, and the latter value is 48.5909. The vector sum of the spin magnetic moments for each type of ion in pure α-MnO_2 is listed in Table 1, and the net magnetic moment of the whole cell is approximated to 0. The net magnetic moment of Fe-doped MnO_2 is calculated to be -0.9995, as shown in Table 1, which further supports the appearance of magnetism. It should be noted that the increased asymmetrical distribution of the DOS for doped MnO_2 is mainly attributed to the contribution of the Fe 3d state. Fe doping introduces spin-polarization around the Fermi level, and hence the net magnetic moment in MnO_2, which results in the magnetic configuration of Fe-doped MnO_2. It is in line with the experimental observations in our previous work.[4] It is supposed that the specific electronic configuration of Fe brings this intriguing magnetic enhancement, which is not observed in Ni/Co-doped MnO_2.[16]

4 Conclusion

In this paper, first-principles calculations are adopted to study the effect of Fe doping on the microwave electromagnetic performance of α-MnO_2 for the first time. The results show that

the covalent bond length of M–O is reduced, while the degree of overlap within the M–O bond is increased after Fe doping, which corresponds to the enhanced bond strength. As a result, instead of being consumed, more electric field energy is stored by the increased potential energy of bonding, which reduces the dielectric loss of MnO_2. The spin-electronic DOS demonstrates that Fe doping enhances the spin-polarization of MnO_2, which is mainly attributed to the contribution of the Fe ions. Fe doping effectively increases the total magnetic moment, and therefore results in the magnetic enhancement of MnO_2. The theoretical prediction concluded from the first-principles calculations corresponds well with the experimentally observed phenomena. The results in this paper provide an early stage exploration of theoretical research on the microwave absorbing properties of MnO_2.

Acknowledgements

The authors acknowledge the support from the National Natural Science Foundation of China [no. 51007005], the National Science and Technology support plan for twelfth five years of China [No: 2012BAJ02B04], and the Fundamental Research Funds for the Central Universities.

References

1 H. T. Guan, Y. B. Zhao, S. H. Liu and S. P. Lv, *Eur. Phys. J.: Appl. Phys.*, 2007, **36**, 235.
2 Y. P. Duan, H. Ma, X. G. Li, S. H. Liu and Z. J. Ji, *Phys. B*, 2010, **405**, 1826.
3 M. Zhou, X. Zhang, J. M. Wei, S. L. Zhao, L. Wang and B. X. Feng, *J. Phys. Chem. C*, 2011, **115**, 1398.
4 Y. P. Duan, H. Jing, Z. Liu, S. H. Li and G. J. Ma, *J. Appl. Phys.*, 2012, **111**, 084109.
5 H. Jing, Y. P. Duan, Z. Liu, J. Zhang and S. H. Liu, *Phys. B*, 2012, **407**, 971.
6 D. H. Park, S. H. Lee, T. W. Kim, S. T. Lim, S. J. Hwang, Y. S. Yoon, Y. H. Lee and J. H. Choy, *Adv. Funct. Mater.*, 2007, **17**, 2949.
7 C. Franchini, R. Podloucky, J. Paier, M. Marsman and G. Kresse, *Phys. Rev. B: Condens. Matter Mater. Phys.*, 2007, **75**, 195128.
8 Q. Wang, Q. Sun, P. Jena and Y. Kawazoe, *Phys. Rev. Lett.*, 2004, **93**, 155501.
9 J. Hafner and D. Hobbs, *Phys. Rev. B: Condens. Matter Mater. Phys.*, 2003, **68**, 014408.
10 E. Cockayne and L. Li, *Chem. Phys. Lett.*, 2012, **544**, 53.
11 J. Zhang, Y. P. Duan, H. Jing and S. H. Liu, *J. Solid State Chem.*, 2011, **184**, 1165.
12 W. N. Li, J. K. Yuan and X. F. Shen, *Adv. Funct. Mater.*, 2006, **16**, 1247.
13 S. Jana, S. Pande and A. K. Sinha, *J. Phys. Chem. C*, 2009, **113**, 1386.
14 S. H. Lee, T. W. Kim, D. H. Park, J. H. Choy, S. J. Hwang, N. Z. Jiang and S. E. Park, *Chem. Mater.*, 2007, **19**, 5010.
15 Y. J. Imai and A. Watanabe, *J. Mater. Sci.: Mater. Electron.*, 2004, **15**, 743.
16 Y. P. Duan, Z. Liu, H. Jing, Y. H. Zhang and S. Q. Li, *J. Mater. Chem.*, 2012, **22**, 18291.
17 S. J. Clark, M. D. Segall, C. J. Pickard, P. J. Hasnip, M. I. J. Probert, K. Refson and M. C. Payne, *Z. Kristallogr.*, 2005, **220**, 567.
18 M. D. Segall, P. J. D. Lindan, M. J. Probert, C. J. Pickard, P. J. Hasnip, S. J. Clark and M. C. Payne, *J. Phys.: Condens. Matter*, 2002, **14**, 2717.
19 A. F. Wright and J. S. Nelson, *Phys. Rev. B: Condens. Matter Mater. Phys.*, 1994, **50**, 2159.
20 J. P. Perdew, J. A. Chevary, S. H. Vosko, K. A. Jackson, M. R. Perderson, D. J. Singh and C. Fiolhais, *Phys. Rev. B: Condens. Matter Mater. Phys.*, 1992, **46**, 6671.
21 H. Ogawa, H. Taketani, A. Kan, A. Fujita and G. Zouganelis, *J. Eur. Ceram. Soc.*, 2005, **25**, 2859.
22 Y. Tsuji, A. Kan, H. Ogawa and S. Ishihara, *J. Eur. Ceram. Soc.*, 2005, **25**, 2883.
23 H. Ogawa, A. Kan, S. Ishihara and Y. Higashida, *J. Eur. Ceram. Soc.*, 2003, **23**, 2485.
24 J. M. Li, Y. X. Han, T. Qiu and C. G. Jin, *Mater. Res. Bull.*, 2012, **47**, 2375.
25 I. D. Brown and R. D. Shannon, *Acta Crystallogr., Sect. A: Cryst. Phys., Diffr., Theor. Gen. Crystallogr.*, 1973, **29**, 266.
26 I. D. Brown and R. D. Shannon, *Acta Crystallogr., Sect. B: Struct. Crystallogr. Cryst. Chem.*, 1976, **32**, 1957.
27 M. G. Brik, *J. Phys. Chem. Solids*, 2010, **71**, 1435.

